



HAL
open science

Dynamics of femtosecond laser absorption of fused silica in the ablation regime

M. Lebugle, N. Sanner, N Varkentina, M. Sentis, O. Uteza

► **To cite this version:**

M. Lebugle, N. Sanner, N Varkentina, M. Sentis, O. Uteza. Dynamics of femtosecond laser absorption of fused silica in the ablation regime. *Journal of Applied Physics*, 2014, 116, pp.063105. 10.1063/1.4892158 . hal-01201866

HAL Id: hal-01201866

<https://hal.science/hal-01201866>

Submitted on 18 Sep 2015

HAL is a multi-disciplinary open access archive for the deposit and dissemination of scientific research documents, whether they are published or not. The documents may come from teaching and research institutions in France or abroad, or from public or private research centers.

L'archive ouverte pluridisciplinaire **HAL**, est destinée au dépôt et à la diffusion de documents scientifiques de niveau recherche, publiés ou non, émanant des établissements d'enseignement et de recherche français ou étrangers, des laboratoires publics ou privés.

Dynamics of femtosecond laser absorption of fused silica in the ablation regime

M. Lebugle, N. Sanner, N. Varkentina, M. Sentis, and O. Utéza

Citation: *Journal of Applied Physics* **116**, 063105 (2014); doi: 10.1063/1.4892158

View online: <http://dx.doi.org/10.1063/1.4892158>

View Table of Contents: <http://scitation.aip.org/content/aip/journal/jap/116/6?ver=pdfcov>

Published by the [AIP Publishing](#)

Articles you may be interested in

[Femtosecond laser ablation dynamics of fused silica extracted from oscillation of time-resolved reflectivity](#)

J. Appl. Phys. **115**, 103504 (2014); 10.1063/1.4867438

[Absorption of a single 500fs laser pulse at the surface of fused silica: Energy balance and ablation efficiency](#)

J. Appl. Phys. **114**, 173105 (2013); 10.1063/1.4829015

[Parallel generation of nanochannels in fused silica with a single femtosecond laser pulse: Exploiting the optical near fields of triangular nanoparticles](#)

Appl. Phys. Lett. **95**, 063101 (2009); 10.1063/1.3186787

[Plasma formation and structural modification below the visible ablation threshold in fused silica upon femtosecond laser irradiation](#)

Appl. Phys. Lett. **91**, 082902 (2007); 10.1063/1.2766848

[Ultrafast double-pulse ablation of fused silica](#)

Appl. Phys. Lett. **86**, 151110 (2005); 10.1063/1.1901806

The logo for the Journal of Applied Physics (AIP) is displayed in a white font on an orange background. The letters 'AIP' are large and bold, followed by a vertical bar and the words 'Journal of Applied Physics' in a smaller font.

Journal of Applied Physics is pleased to announce **André Anders** as its new Editor-in-Chief

Dynamics of femtosecond laser absorption of fused silica in the ablation regime

M. Lebugle,^{a)} N. Sanner, N. Varkentina, M. Sentis, and O. Utéza
 Aix Marseille Université, CNRS, LP3 UMR 7341, 13288 Marseille, France

(Received 16 May 2014; accepted 24 July 2014; published online 13 August 2014)

We investigate the ultrafast absorption dynamics of fused silica irradiated by a single 500 fs laser pulse in the context of micromachining applications. A 60-fs-resolution pump-probe experiment that measures the reflectivity and transmissivity of the target under excitation is developed to reveal the evolution of plasma absorption. Above the ablation threshold, an overcritical plasma with highly non-equilibrium conditions is evidenced in a thin layer at the surface. The maximum electron density is reached at a delay of 0.5 ps after the peak of the pump pulse, which is a strong indication of the occurrence of electronic avalanche. The results are further analyzed to determine the actual feedback of the evolution of the optical properties of the material on the pump pulse. We introduce an important new quantity, namely, the duration of absorption of the laser by the created plasma, corresponding to the actual timespan of laser absorption by inverse Bremsstrahlung. Our results indicate an increasing contribution of plasma absorption to the total material absorption upon raising the excitation fluence above the ablation threshold. The role of transient optical properties during the energy deposition stage is characterized and our results emphasize the necessity to take it into account for better understanding and control of femtosecond laser-dielectrics interaction. © 2014 AIP Publishing LLC. [<http://dx.doi.org/10.1063/1.4892158>]

I. INTRODUCTION

The study of ultrafast absorption in dielectrics is of key interest for fundamental investigations in the framework of femtosecond laser micromachining. Numerous applications are based on the interaction of femtosecond pulses with transparent materials, among which micro-fabrication with nano-scale features, glass processing for consumer electronics or laser surgery.¹⁻⁴ For the best control of such processes, it is important to provide no more than the amount of laser energy necessary to machine the calibrated modification of the material surface, in order to limit the laser-induced stress and to avoid a degradation of the quality of the outcome.⁵ Dielectric materials being initially transparent to near infrared laser light, non-linear absorption mechanisms⁶ are required to bridge the band gap and promote free electrons in the conduction band.^{7,8} These seed electrons are further accelerated through inverse Bremsstrahlung (IB) and multiplied by impact ionization if their kinetic energy is sufficient, leading to an avalanche multiplication phenomenon. Strong laser absorption therefore takes place in the first hundred nanometers at the surface of the material, where the material has been turned opaque. It may yield to damage or ablation of the material, if the quantity of laser energy absorbed by the material is sufficiently high and properly adjusted.^{9,10} At densities higher than the critical density, a plasma mirror effect affects the propagation by reflecting part of the pulse. Knowledge of the transient optical properties of the material submitted to laser exposure is thus of paramount importance to achieve such objective of fine control of the laser absorption process.

Measurements of transient optical properties of dielectrics irradiated by femtosecond pulses were previously reported and analyzed in link with the ablation process.¹¹⁻¹⁵ Other works focused more on the time-integrated energy deposition stage and on fundamental ionization mechanisms.¹⁶⁻¹⁸ Numerical modeling also gave insights on the details of the interaction,¹⁹⁻²² especially yielding information on the time-dependent reflectivity and transmissivity, and thus on the absorption dynamics. While the qualitative picture of ultrafast evolution of the optical properties is rather clear in the actual understanding of the interaction, their actual characteristics at the pulse timescale and the consequences on the laser energy deposition still remain to be clarified experimentally.

In this work, we investigate the dynamics of absorption of fused silica during the excitation pulse. To this aim, we develop a degenerate pump-probe setup at 1025 nm with a high temporal resolution (Sec. II). The dynamics of the plasma induced by the pump at the surface of the material is probed with a 60 fs pulse, much shorter than the 500 fs pump pulse. This makes feasible a direct observation of transient optical properties with retrieval of plasma absorption, with high optical sampling (Sec. III). The estimation of the magnitude and the dynamics, with which the photons of the pump pulse are absorbed once the plasma has been generated, then becomes possible. We further introduce and extract from our data an important new quantity, which is the duration of plasma absorption (Sec. IV). It gives insights on the strength of this mechanism and evidences various interaction regimes as a function of the incident fluence. This yields a comprehensive characterization of the dynamics of the interaction in the regime of ablation.

^{a)}Author to whom correspondence should be addressed. Electronic mail: lebugle@lp3.univ-mrs.fr

II. EXPERIMENTAL SETUP

A non-collinear, degenerate, and orthogonally polarized pump-probe experiment is developed to determine the time-resolved absorption at the pulse timescale (Fig. 1(a)). The surface of the SiO₂ sample is exposed to a single pump pulse (1025 nm, 500 fs, 60 μJ, emitted by a Yb : KGW laser source from Amplitude Systèmes) at normal incidence with horizontal polarization, and probed by a s-polarized pulse

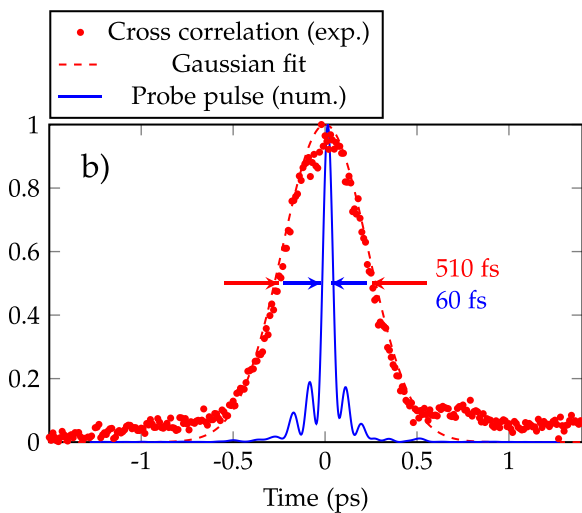
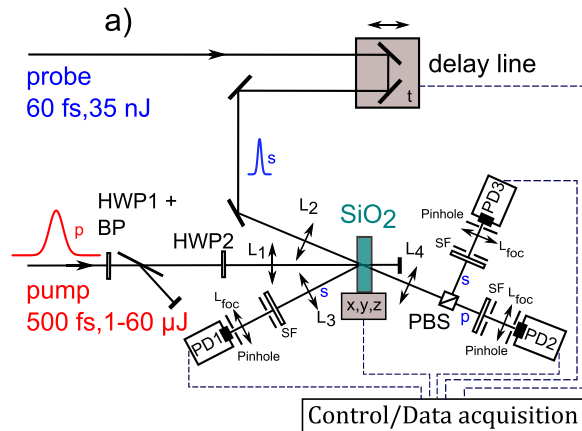


FIG. 1. (a) Schematic layout of pump-probe setup. HWP: Half-Wave Plate; BP: Brewster Polarizer; L₁, L₂: pump and probe focusing lenses with focal lengths $f_1 = 75$ mm and $f_2 = 50$ mm; L₃, L₄: probe recollimating lenses with focal lengths $f_3 = f_4 = 50$ mm; PD1-3: Si-photodiodes; SF: Spectral and spatial Filters; PBS: Polarizing Beam Splitter. L_{foc}: probe focusing lenses with focal lengths $f_{foc} = 25$ mm. Pinholes are placed in the focal plane of L_{foc} to minimize the noise and also, considering the case of the reflected signal, to isolate the signal coming from the front face of the sample from the back face one. The two beams at the same wavelength are superimposed spatially at the surface of the sample with an angle of 20°. Photodiodes 1 and 3, respectively, integrate the reflectivity and transmissivity of the probe pulse. Photodiode 2 is used for 3rd order cross-correlation and determination of the time origin (zero time-delay). The Half-Wave Plate HWP2 is used in the X-FROG experiment to adjust the pump polarization in order to define the zero time delay. To preserve the zero time delay between the pump and probe pulses in the experiments, HWP2 is rotated to provide p-polarized pump onto the target. (b) Temporal shapes of 3rd order cross-correlation signal (between pump and probe) and probe pulse (retrieved from FROG trace), demonstrating the high temporal resolution achieved in this experiment. Note that the convolution trace between pump and probe is close to the retrieved pulse trace (with FWHM of 500 fs assuming Gaussian distribution) from an independent measurement of 2nd order autocorrelation (APE-Mini).

(1025 nm, 60 fs) at an angle of 20°. A Pockels cell and a polarizing beam splitter are used for picking single-shot pulses from the 1 kHz pulse train. The beam is split into two arms for providing the pump and probe beams. The probe pulse undergoes self-phase modulation in a photonic crystal fiber that broadens its spectrum, which finally reaches 30 nm at FWHM. It is further compressed by chirped mirrors leading to the delivery of 60 fs pulses. Characterization of the probe pulse is obtained through Polarization-Gated X-FROG technique²³ (cross Frequency Resolved Optical Gating) performed at the surface of the sample positioned in the focal plane of the two beams. This arrangement takes advantage of the third-order non-linearity of the SiO₂ sample under investigation (non-linear index: $n_2 \approx 3 \times 10^{-16}$ cm²/W). It exploits the pump-induced positive change of the index of refraction (Kerr effect) triggered by the incident intensity in the range of 10¹² W/cm². This induces a delay-dependent birefringence of the medium, since the Kerr effect only occurs along the polarization axis. For this measurement, the pump p-polarization is previously rotated of 45° with a half-wave plate (HWP2 in Figure 1(a)) so that the electric field of the probe pulse is oriented at 45° with respect to that of the pump pulse. As a result, the fused silica sample acts as a wave plate while the pump pulse is present, slightly rotating the polarization of the probe pulse; therefore, an orthogonal p-polarized probe signal is detected by PD2. The extinction ratio of the polarizers used is higher than 1000 : 1 (Thorlabs, Nanoparticle Linear Film Polarizer, LPNIR).

The FROG trace is obtained after recording at each delay the spectrum of the p-component by a spectrometer (Avantes, AvecSpec-Mini) located at the place of PD2. Using a FROG reconstruction algorithm software (Femtosoft Technologies, LLC), we retrieve the temporal intensity and phase of the probe pulse. Fig. 1(b) shows the cross-correlation trace, obtained by extracting the FROG time-marginal, that is, the temporal intensity distribution (510 fs at FWHM) of the pump pulse convoluted by the shorter probe. The numerically retrieved probe pulse is also shown, with 60 fs at FWHM, leading to a ratio of durations $\tau_{pump}/\tau_{probe} \approx 8$. Using this technique has two major advantages for our study: (i) the temporal characterization is performed with the same sample that is used for pump-probe experiments and (ii) zero time-delay (temporal superposition of the peaks of probe and pump pulses) is determined very easily and does not need any additional experimental adjustment, thus limiting the systematic uncertainty on the synchronization of the probe and pump pulses. After this measurement, the pump polarization is turned back to p-polarization with HWP2, to ensure crossed pump and probe polarizations. The time resolution of the pump-probe measurement is estimated to be 60 fs (duration of the probe at FWHM), making possible a high optical sampling in the following experiments. Note that the impact of the angle (20°) used in the non-collinear geometry of the experiment is negligible on the temporal resolution as it can be estimated elsewhere.²⁴

To investigate the formation and dynamics of the electron-hole plasma, we perform time-resolved measurements of reflectivity and transmissivity at the surface of the sample. The sample consists of 2.5 mm thick disks of high-purity

amorphous SiO₂ (Suprasil by Heraeus, band gap of 8.9 eV), and with impurity lower than 0.065 ppm; total bubble cross section within the volume is 0.015 mm²/100 cm³. The sample is super-polished with a residual roughness measured with an AFM (Atomic Force Microscopy) of $R_a = 0.2$ nm. The pump beam with a nearly Gaussian intensity distribution is focused at normal incidence with a lens of focal length $f_1 = 75$ mm on the sample surface, leading to spot radii of $(14.5 \times 13.8) \mu\text{m}^2$ at $1/e^2$. The probe beam is focused with focal $f_2 = 50$ mm leading to spot radii of $(12.0 \times 11.3) \mu\text{m}^2$ at $1/e^2$. Considering the 20° angle of incidence, the two beams therefore exhibit almost the same dimensions.

The beams are furthermore carefully experimentally superimposed, by double checking through: (i) *in-situ* imaging with $\sim \mu\text{m}$ spatial resolution and (ii) monitoring of the level of change in the probe signals. All experiments are performed under ambient air. The spacing between adjacent irradiated sites is 75 μm , preventing any contamination by possible redeposition of debris in a neighbor impact.

The pump fluence delivered on the sample is varied with an association of a half-wave plate (HWP1) and a Brewster polarizer. Note that the laser fluence F is always expressed considering the peak fluence $F = 2E/\pi\omega_0^2$. For that calculation, we take the average of the beam waists measured along the two axes. After interaction, the energy of the reflected and transmitted probe pulses are measured for each delay time at the location of PD1 and PD3, respectively, and then normalized to their values at rest. To minimize the noise, long pass cut-on spectral filters at 950 nm are implemented for optical isolation of the signals with respect to the broadband plasma emission. Pinholes with weakly closed apertures are also added after recollimation to minimize contributions coming from solid angles much larger than the probe beam one. Finally, as we are precisely interested in the energy deposition process, only data up to a few picoseconds before and after the pump peak are shown here.

III. TIME-RESOLVED PLASMA PROPERTIES

A. Data handling

Optical properties are measured as a function of time delay for a set of increasing fluences. As we concentrate here on the ablation regime, the laser-induced ablation threshold $F_{th,LIAT}$ is first measured with a dedicated procedure.²⁵ Briefly, it is defined as the linear extrapolation of the crater volumes to zero for decreasing fluences (confocal microscopy measurements with averaging over 5 craters for each fluence). We obtain $F_{th,LIAT} = 5.8 \text{ J/cm}^2$. In the following experiments, the pump fluence is varied from $0.8F_{th,LIAT} = 4.6 \text{ J/cm}^2$ up to $3.9F_{th,LIAT} = 22.6 \text{ J/cm}^2$.

For fluences below the threshold, no significant variations of the probe signals are recorded, whereas for all fluences higher than the ablation threshold the plasma properties strongly evolve during the pulse. Note that we use a low-intensity probe pulse, whose intensity $I_{probe} \approx 2 \times 10^{11} \text{ W/cm}^2$ is well below any material modification threshold for a 60 fs pulse. Indeed, we verified that no depletion of the probe pulse occurs when the pump beam is blocked. We also experimentally checked that no change is

observable in the response of the plasma as a function of the probe energy. Thus, the plasma absorption read by the probe mainly corresponds to absorption by IB that means the heating of the free carriers (produced by the pump pulse) through collisions of a photon with an electron in the field of the parent atom. The magnitude of this one-photon absorption of the probe is then directly representative of the free electron density of the plasma.

The results of reflectivity $R(t)$, transmissivity $T(t)$, and absorptivity $A(t)$ are shown on Fig. 2 for three cases above the threshold ($1.2F_{th,LIAT}$, $1.5F_{th,LIAT}$, and $3.9F_{th,LIAT}$). The pump pulse intensity is shown on the secondary axis to correlate the plasma dynamics with the excitation. Each data point represents the measured reflectivity and transmissivity of a single laser pulse. Without excitation, $R_0 = 4.0\%$ and $T_0 = 96.0\%$ are given by the Fresnel equations for a s-polarized probe at an angle of 20°. As the sample is thick, we do not measure the reflection related to the second face of the sample, which implies a small bias on the extraction of the evolution of the absorption. This bias is maximum (and equal to 4%) when the pulses experience a low-density plasma allowing high transmission. It is expected to decrease at high excitation when the material turns absorbing during the laser pulse (low transmission). For sake of simplicity and as this bias is not significant, we thus ignore the reflection loss onto the second face of the sample. We further infer the absorptivity using $A = 1 - R - T$. Note that to retrieve the absorptivity A , we assume that the light scattered by the material under irradiation has no influence at this timescale. This point is confirmed by two independent observations. First, the low numerical aperture used here ($N.A. \approx 0.03$) leads to a relatively large focal spot producing a nearly homogeneous plasma transversely in the probed zone, preventing scattering in all directions. Second, another time-resolved measurement by Rosenfeld *et al.* indicates that significant scattering due to the onset of plasma expansion only occurs after time $t > 2 - 3 \text{ ps}$.²⁶ Finally, as an illustration, Figures 2(d), 2(h), and 2(l) show microscope images of the craters obtained with fluences $1.2F_{th,LIAT}$, $1.5F_{th,LIAT}$, and $3.9F_{th,LIAT}$.

B. Plasma reflection

Figs. 2(a), 2(e), and 2(i) show a rise of the level of reflectivity with increasing fluence. Temporally, the curves present a sharp increase in the second half of the pump pulse. A saturation is attained after the pulse at a time delay around 0.5 ps for all fluences, e.g., $R \approx 4R_0 = 16\%$ at a fluence of $3.9F_{th,LIAT}$. The reflectivity of the probe only depends on the evolution of the dielectric function at the surface of the sample, implying the contribution of the first atomic outer layers of the surface which are progressively turned into a highly absorbing free electron-hole plasma by the laser excitation. Assuming homogeneous distribution of free-electron density in the spatial layers inducing the reflection, a simple punctual estimation of the surface reflectivity can be made with the Drude model coupled to the Fresnel equations. The complex dielectric function ϵ_t is determined by the mutual contributions of the unexcited solid and the free electron gas with density n_e ,^{27,28}

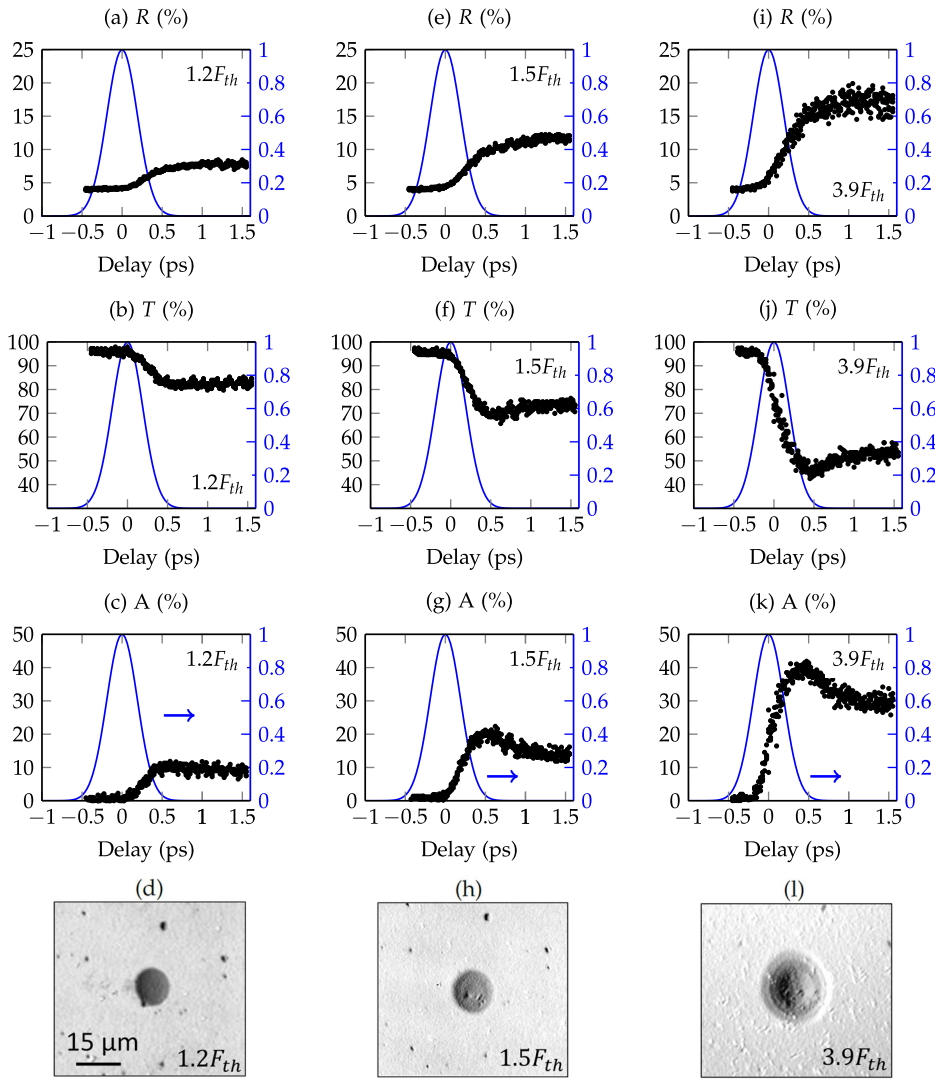


FIG. 2. Reflected ((a), (e), and (i)), transmitted ((b), (f), and (j)), and absorbed ((c), (g), and (k)) energy fractions at short timescale ($-0.5 \text{ ps} < t < 1.5 \text{ ps}$) as a function of pump-probe time delay for $F = 1.2F_{th,LIAT}$ (first column), $F = 1.5F_{th,LIAT}$ (second column), and $F = 3.9F_{th,LIAT}$ (third column), respectively. In (d), (h), and (l) are shown the corresponding microscope images of the craters for illustration. No significant variations of the probe signals were observed for fluences below the threshold. The normalized pump pulse intensity is shown on the secondary axis (blue line). The time resolution is 60 fs.

$$\epsilon_t = \epsilon_i - (\epsilon_i - 1) \frac{n_e}{n_{at}} - \frac{\omega_p^2}{\omega_l(\omega_l + i/\tau_e)}, \quad (1)$$

where $\epsilon_i = 2.1$ is the dielectric constant of unexcited SiO_2 at 1025 nm, $n_{at} = 2.2 \times 10^{22} \text{ cm}^{-3}$ is the valence band density corresponding to single molecular ionization, ω_l is the laser frequency, $\omega_p = \sqrt{n_e e^2 / (m_e \epsilon_0)}$ is the plasma frequency with e and m_e are the electron charge and mass, and ϵ_0 is the dielectric permittivity of vacuum. In approximation, we take the effective electronic collision time equal to: $\tau_e = 1.7 \text{ fs}$.²⁹ The effective electronic collision time is indeed varying as a function of the free electron density and temperature.³⁰ We chose the value given above as it was inferred from experiments performed on SiO_2 at similar intensities. Note also that we neglect the term related to the Kerr effect in the expression of the complex dielectric function (see Eq. (1)). Indeed, in the regime of ablation of dielectrics, it can be omitted since the predominant contributions in the dielectric function are related to the creation of free electron population upon laser excitation (second and third right-hand terms in Eq. (1)). In addition, as we are interested here in evaluating the skin depth at the maximum of the reflectivity (attained around 0.5 ps), the optical Kerr effect is expected to be negligible as this time corresponds to the end of the pulse.

The Fresnel equations for s-polarized light at 20° incidence give the intensity reflection coefficient R_s . The skin depth l_{abs} , defined with respect to the laser intensity, is calculated with $l_{abs} = c / (2\omega_l \kappa)$, where $\kappa = \text{Im}(\sqrt{\epsilon_t})$ is the imaginary part of the complex refractive index. A positive variation of the reflectivity indicates that the electron density locally exceeds the critical density, $n_{cr} = 1.06 \times 10^{21} \text{ cm}^{-3}$ at our wavelength. We can then estimate the electron density in a thin layer beneath the surface. For the reflectivity maximum of $R \approx 16\%$ attained around 0.5 ps with a fluence of $3.9F_{th,LIAT}$ (see Fig. 2(i)), the electron density reaches $n_e \approx 3 \times 10^{21} \text{ cm}^{-3}$. This evidences the formation of an overdense plasma during the excitation pulse. The transient skin depth is then of the order of $l_{abs} \approx 100 \text{ nm}$.

Note that this very simple estimation holds for what happens on the laser axis only. Besides, the experiment is performed with Gaussian beams, and the R , T , and A coefficients are integrated over the whole areas of the beams. Therefore, the local value of R at the beam center is probably higher, and so does the electronic density, which should in reality reach values above the one estimated here.

With respect to the time dynamics of the reflectivity, we observe a saturation of the reflectivity for three cases of fluence presented here. A peculiar time delay of $\approx 0.5 \text{ ps}$ is

necessary to reach the reflectivity maximum (see Figs. 2(a), 2(e), and 2(i)), which corresponds to the time to significantly heat the free electron population through IB to yield impact ionization and further avalanche. Even after the excitation pulse, a slight increase of the electron density at the surface is seen. Such a delay was previously reported by Puerto *et al.*,¹³ with 800 nm excitation and 400 nm detection light. With our higher temporal resolution and degenerate experiment at 1025 nm, we confirm here this order of magnitude of time necessary to reach the maximum electron density at the surface. We interpret this behavior as a sign of significant electronic avalanche, since no photoionization can take place in the absence of the pump pulse, but only impact ionization. At a delay of ~ 0.5 ps, the electronic density is thus maximal.

Longer timescale measurements (not shown here) evidence that this high level of reflectivity stays constant until 5 ps, revealing that an overcritical electron population remains free in a thin depth beneath the surface at picosecond timescale and that it is therefore not subjected to losses or exciton trapping mechanisms. After a time delay of 5 ps, it becomes too complex to investigate precisely its dynamics since other effects related to the energy transfer to the lattice, hydrodynamic plasma expansion, and thermodynamic phase transitions take place.

C. Plasma transmission

The curves of time-resolved transmission of the plasma during the pump pulse are reported on Figures 2(b), 2(f), and 2(j). The information recovered by the transmitted signal is different and complementary to the reflectivity. Indeed, the transmitted beam probes the entire thickness of the sample and thus contains information concerning both the surface and the bulk of the sample, resulting from an average measurement along the Rayleigh length of the probe beam ($\approx 550 \mu\text{m}$). Thus, simple analytical models do not hold anymore. However, a careful comparison between the two different dynamics of R and T allows us to retrieve qualitative information.

The transmissivity experiences a decrease, starting earlier upon increase of the fluence. Moreover, we observe a fast and sharp drop, especially at the highest fluence of $3.9F_{th,LIAT}$, that begins temporally slightly earlier than the reflectivity rise (by comparison with Fig. 2(i)). Whatever the fluence, the transmissivity reaches a minimum (whose value depends on the applied fluence) that is attained at ~ 0.5 ps, i.e., roughly at the end of the pulse. A slight recovery is even observed afterwards for the highest fluence case, nevertheless stabilized after 1 ps. The origin of this recovery remains actually unclear. We possibly attribute this behavior to defocusing of the probe provoked by the high electron density reached at the very end of the pump pulse. According to Rae,³¹ the phase change over the length l_{abs} can be approximated by $\Delta\varphi = (\pi l_{abs}/\lambda)(n_e/n_{cr})$, a phase change of $\pi/2$ corresponding to a doubling of the diffraction-limited beam divergence. In our excitation condition of $3.9F_{th,LIAT}$, we obtain $\Delta\varphi \approx \pi/3$, corresponding to a significant increase of the divergence of the probe. As a result, the probed volume

also includes a contribution of less-dense plasma regions surrounding the central part of the excited zone, yielding a weak recovery of transmissivity. Note that this fine detail of the interaction is revealed thanks to the high temporal resolution of our pump-probe experiment.

D. Plasma absorption

We now combine the reflectivity and transmissivity data to investigate absorption properties of the plasma (Figs. 2(c), 2(g), and 2(k)). A sharp increase occurs during the pulse and the absorptivity reaches a maximum at time 0.5 ps, e.g., around 35% – 40% for $3.9F_{th,LIAT}$ (see Fig. 2(k)), corresponding to a maximum of the electron density reached in average along the path of the transmitted beam. Like reflectivity and transmissivity signals, the absorptivity starts rising earlier for increasing fluences. Now, the precise knowledge of this time-resolved plasma absorption is used in the following to finely characterize the duration of the fraction of the pump pulse that is absorbed by the plasma through IB mechanism.

IV. RETRIEVAL OF PUMP ABSORPTION

A. Plasma absorption at the pulse timescale

Our results show that the transient optical properties of the laser-induced plasma determine the temporal shape of energy deposition in matter which is initially transparent at the laser wavelength. Thus, we now aim at establishing a precise energy balance for the plasma at the timescale of the pump pulse. We use the time-resolved absorptivity measured by the probe and multiply it by the temporal pump intensity to retrieve the absorption seen by the pump pulse as a function of time. This data treatment is indeed valid thanks to the caution we have paid to the superimposition of the probe and pump beams, and also of course because pump and probe have the same wavelength. A slight error is expected by inferring the optical properties of the pump beam, at normal incidence, from those seen by the probe beam, with 20° incidence. We have calculated the expected variation of absorption probed by two beams positioned at these angles considering large variations of the dielectric function in the complex plane with the Eq. (1) coupled to the Fresnel equations. The maximum variation is of the order of $\pm 3\%$ and, thus, it can be considered as negligible. Hence, the propagation of the pump pulse, which is affected as a function of time by the self-generated plasma, is closely driven and described by the plasma optical properties previously measured. Non-linear effects occurring during the pump pulse propagation in SiO_2 , such as multiphoton absorption or Kerr effect, as well as non-linear spatio-temporal reshaping of the pump beam related to the short pulse duration, are not accounted for with this experiment. In our maximum excitation conditions ($3.9F_{th,LIAT}$), the peak power is ≈ 0.14 GW (corresponding intensity of $4.5 \times 10^{13} \text{ W/cm}^2$) yielding a self-focusing distance³² in SiO_2 of $\approx 40 \mu\text{m}$ ($P_{cr} \approx 3.1 \text{ MW}$ at 1025 nm)³³ much larger than the skin depth. The peak power is also sufficiently low to prevent any self-focusing or ionization in air prior the target. So, in first approximation,

the influence of such non-linear effects before and in the target can be neglected. Multiphoton absorption that yields the initial depletion of the pump pulse and turns the material from a transparent to an absorbing state is not measured in this experiment but this effect is expected to have no significant influence on the phase of the pump pulse and thus on the way it propagates. Then, the corresponding reflected, transmitted, and absorbed pump pulse intensities resulting from the interaction with the plasma are calculated by

$$\begin{aligned} I_{R,p}(t) &= R(t) \cdot I_p(t), \\ I_{T,p}(t) &= T(t) \cdot I_p(t), \\ I_{A,p}(t) &= A(t) \cdot I_p(t), \end{aligned} \quad (2)$$

where $R(t)$, $T(t)$, and $A(t)$ are the measured optical properties of the plasma as a function of time delay t , and $I_p(t) \propto \exp[-4\ln 2(t/\tau)^2]$ is the time intensity of the pump, with $\tau = 500$ fs.

Fig. 3 shows the time evolution of the instantaneous reflected, transmitted, and absorbed intensities of the pump pulse normalized to the peak intensity, in the case of the highest fluence $3.9F_{th,LIAT}$. A significant alteration of pump propagation is triggered just before the peak pulse, around $t = -100$ fs and mostly occurs during the second part of the pulse, for $t > 0$. The transmission is suddenly cut-off due to strong absorption of the peak pulse by the plasma, which is maximal around $t = +100$ fs.

To quantify the plasma response, we integrate and normalize the intensities over time to obtain the fractions of reflected (η_R), transmitted (η_T), and absorbed (η_A) energy, resulting from the interaction of the pump pulse with the plasma. For $3.9F_{th,LIAT}$, we obtain $\eta_R \approx 8\%$, $\eta_T \approx 73\%$; the absorbed fraction is therefore of the order of $\eta_A \approx 20\%$. The plasma mirror effect, leading to a reflection coefficient that reaches twice the value at rest, has an impact on the laser energy balance but it is rather limited. Nevertheless, it is

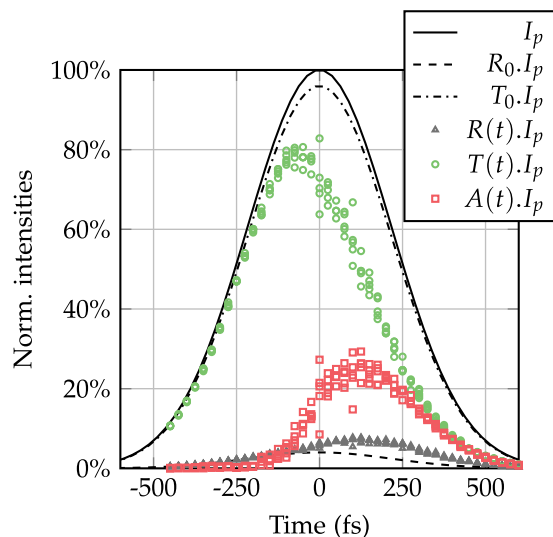


FIG. 3. Transmitted (green circles), reflected (grey triangles), and absorbed (red squares) intensity fractions of the pump pulse resulting from the interaction with the plasma at $3.9F_{th,LIAT}$. The black dashed and dashed-dotted lines indicate the reflectivity and transmissivity of SiO_2 at rest, respectively.

important to note that the presence of an overcritical plasma dramatically affects the interaction dynamics by strongly localizing the deposition of the incident energy in the skin depth.

The important role of the fluence level is highlighted by comparing the absorbed fractions at $3.9F_{th,LIAT}$ ($\eta_A \approx 20\%$) and $1.2F_{th,LIAT}$ ($\eta_A \approx 2\%$). While the incident energy is increased ≈ 3 times, a 10-fold variation in this amount of energy absorbed by the plasma is put in evidence. This variation is seen in the large increase of the corresponding ablated depths observed in these two ablation conditions (≈ 65 nm and ≈ 300 nm for $1.2F_{th,LIAT}$ and $3.9F_{th,LIAT}$, respectively, see also Figure 2). Afterwards, the knowledge of η_A , which is directly representative of the plasma layer characteristics (especially its axial gradient) would therefore be of great help as an experimental input for further modeling of femto-second pulses interacting with dielectrics.

B. Duration of plasma absorption as a function of fluence

Our experiments finally offer the possibility to evaluate the duration of absorption of the pump pulse by the plasma, that is, the energy solely acquired by IB that further triggers avalanche. Using an arbitrary criterion of 2% of pump absorption ($I_{A,p}(t) > 2\%$), we therefore introduce the onset time t_o and the end time t_e of plasma absorption of the pump pulse. The duration of absorption is simply calculated with $\Delta t_{abs} = t_e - t_o$. Note that the chosen criterion is significantly higher than the measurement noise, and taking another value in the range of percent would not affect the inferred conclusions. Fig. 4 shows the onset and the duration of plasma absorption for increasing fluence. For example, at a fluence of $1.2F_{th,LIAT}$, this criterion is exceeded during approximately 225 fs, starting at time +150 fs, thus clearly occurring during the second half of the pulse. As the fluence increases, plasma absorption starts earlier and its duration dramatically increases up to 650 fs, which represents the most of the pulse. The inset of Fig. 4 shows the onset time t_o as a function of fluence. The onset time is +150 fs after the pulse

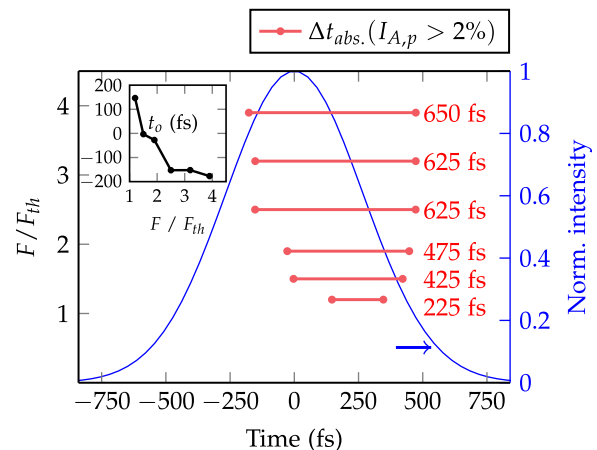


FIG. 4. Duration of the plasma absorption, defined as the time interval such as the pulse absorption exceeds a fixed criterion (2%) for increasing normalized fluence. The pulse temporal profile is shown on the secondary axis (blue line). Inset: dependence of the onset time t_o on the normalized fluence.

peak for low excitation levels and shortens with increasing fluence until reaching a saturation level of approximately -200 fs prior to the pulse peak.

With respect to the physical meaning of this duration, we now suggest the following picture. Plasma absorption occurs only at the very end of the pulse and during a short period of time for a pump fluence close to the threshold. This means that most of the photons are probably absorbed by multiphoton processes, without significantly triggering impact ionization. This is supported by the fact that no plasma absorption was observed below the ablation threshold, as already mentioned in Sec. III. On the opposite, the plasma absorption starts early in the pulse and lasts almost the whole pulse length at high fluence. Hence, we observe a strong contribution of plasma absorption that compares favorably with the occurrence of an electron avalanche process. This is in agreement with our previous comment on the significant delay of 0.5 ps necessary to reach the electron density maximum at the surface. Furthermore, we interpret the saturation of the onset time t_o around -200 fs as the minimal time required to generate a strongly absorbing plasma by non-linear ionization. The fraction of energy of the leading edge of the pulse, that propagates in a transparent medium, was actually measured experimentally¹⁸ as well as predicted numerically²² and corresponds to the picture proposed here.

We therefore show that a transition takes place from the low-fluence regime dominated by the multiphoton absorption to the high-fluence regime dominated by the plasma absorption mostly confined in the skin depth. This evolution of the respective importance of the absorption channels as a function of fluence is of high importance for fundamental plasma studies as well as for micro-machining applications. For technological purposes, it emphasizes the difficulty to choose the appropriate energy input to obtain the best compromise between ablation efficiency, in terms of units of volume removed per incident photon, and minimal incident fluence to avoid an excess of absorbed energy that may degrade the final result. We recently showed that, even at a moderate fluence around $3F_{th,LIAT}$, an important excess of energy is deposited with respect to that required for ablation.¹⁸ A fluence range for optimal ablation efficiency, in same operating conditions, was suggested around $2F_{th,LIAT}$. With respect to the present work providing quantitative information on the dynamics of energy deposition, we additionally observe that this excitation level corresponds to a particular situation. With incident fluence in the range of 1.5 to $2F_{th,LIAT}$, the onset time t_o is very close to zero (see inset of Fig. 4). This means that the pulse peak, carrying most of the energy, can be very efficiently absorbed by the plasma generated by the leading edge of the pulse. Qualitatively, it provides a large amount of laser energy to be coupled to the plasma at the optimal moment, since screening effects are still rather low (see Fig. 2(e) for $1.5F_{th,LIAT}$) and arrive later, in the second temporal part of the pulse. Finally, we add that clever handling of such energetic constraints can also be achieved by working somewhat at lower fluences and using a second pulse delayed in time. In our conditions (or similar), a delay of $+500$ fs is probably optimal in order to take advantage of

the maximum plasma absorption (see Fig. 2(k)). This is consistent with the work presented in Ref. 34, in which an increase of the ablation efficiency on fused silica is observed when temporally asymmetric pulse trains are used, with decreasing intensity envelope and a separation of 500 fs between each maximum intensity. Another strategy would be to synthesize a temporally shaped single pulse composed of a steep and intense leading edge followed by a long plateau with weaker power.

Looking forward, taking into account these considerations arising from the temporal dynamics would allow to gain control on the energy deposition stage of sub-picosecond laser pulses. This is particularly interesting for applications requiring precise and efficient ablation of dielectrics at the micrometer scale.

V. CONCLUSION

We have experimentally investigated with a high sampling resolution the temporal response of SiO_2 irradiated by a single sub-picosecond laser pulse. The dynamics of the electron-hole plasma has been analyzed through the evolution of its optical properties. Our results reveal the presence above the threshold of an overcritical electron-hole plasma with density higher than 10^{21} cm^{-3} at picosecond delays, localized in a thin depth of the material under the surface. We also observed an important delay of approximately 0.5 ps necessary to reach the maximum electron density at the surface that compares favorably with the occurrence of retarded avalanche ionization.

Moreover, our experiments make possible to correlate the plasma optical properties to the pulse propagation. The plasma mirror effect has a moderate impact, with an overall reflection coefficient that remains of the order of 10% in our experimental conditions up to $\sim 4F_{th,LIAT}$. Finally, the high resolution achieved in this experiment allows us to precisely retrieve the duration of pump absorption by the plasma. Through its evolution as a function of fluence, and considering the question of laser energy coupling into a dielectric material, our results evidence the transition from the low-fluence regime dominated by the multiphoton absorption to the high-fluence regime dominated by the plasma absorption through inverse Bremsstrahlung mechanism and avalanche phenomenon.

We also show that a careful choice of the incident fluence promotes a large coupling of the incoming laser energy to the excited material. In this optimal interaction regime ($F \sim 2F_{th,LIAT} \approx 11 \text{ J/cm}^2$), the duration of efficient laser energy deposition in the plasma created at the surface of the material is roughly equal to the FWHM pulse duration, but taking place mostly in the second half of the pulse. In this regime, the screening effects are still rather low, which favors a good consumption of the incident laser energy. Note also that this optimal fluence is consistent with our former observations performed in similar operating conditions.¹⁸

This work is of particular importance in the context of micromachining process, for which a better control of the material excitation is sought. Our results highlight the crucial role of transient optical properties during the laser-matter

interaction in the regime of ablation, and open a comprehensive way toward designing dedicated user-defined temporal excitation profiles.

ACKNOWLEDGMENTS

Financial support of the French National Agency of Research (ANR) - Nanomorphing-07-BLAN-0301-03 and the Region Provence-Alpes-Côte d'Azur and Department of Bouches-du-Rhône is gratefully acknowledged. We also thank Professor E. Gamaly and Professor A. Rode for valuable discussions.

- ¹H. Misawa and S. Juodkazis, *3D Laser Microfabrication: Principles and Applications* (John Wiley & Sons, Hoboken, NJ, USA, 2006).
- ²S. H. Chung and E. Mazur, *J. Biophotonics* **2**(10), 557 (2009).
- ³M. D. Perry, B. C. Stuart, P. S. Banks, M. D. Feit, V. Yanovsky, and A. M. Rubenchik, *J. Appl. Phys.* **85**, 6803 (1999).
- ⁴K. Sugioka and Y. Cheng, *Light: Sci. Appl.* **3**, e149 (2014).
- ⁵A. Ben-Yakar and R. L. Byer, *J. Appl. Phys.* **96**, 5316 (2004).
- ⁶L. V. Keldysh, *Sov. Phys. JETP* **20**, 1307 (1965).
- ⁷B. C. Stuart, M. D. Feit, S. Herman, A. M. Rubenchik, B. W. Shore, and M. D. Perry, *Phys. Rev. B* **53**, 1749 (1996).
- ⁸E. G. Gamaly, A. V. Rode, B. Luther-Davies, and V. T. Tikhonchuk, *Phys. Plasmas* **9**(3), 949 (2002).
- ⁹T. Jia, Z. Xu, R. Li, D. Feng, X. Li, C. Cheng, H. Sun, N. Xu, and H. Wang, *J. Appl. Phys.* **95**(9), 5166 (2004).
- ¹⁰B. Chimier, O. Utéza, N. Sanner, M. Sentis, T. Itina, P. Lassonde, F. Légaré, F. Vidal, and J.-C. Kieffer, *Phys. Rev. B* **84**, 094104 (2011).
- ¹¹I. H. Chowdhury, A. Q. Wu, X. Xu, and A. M. Weiner, *Appl. Phys. A* **81**, 1627 (2005).
- ¹²S. W. Winkler, I. M. Burakov, R. Stoian, N. M. Bulgakova, A. Husakou, A. Mermillod-Blondin, A. Rosenfeld, D. Ashkenasi, and I. V. Hertel, *Appl. Phys. A* **84**(4), 413 (2006).
- ¹³D. Puerto, J. Siegel, W. Gawelda, M. Galvan-Sosa, L. Ehrentraut, J. Bonse, and J. Solis, *J. Opt. Soc. Am. B* **27**, 1065 (2010).
- ¹⁴J. Hernandez-Rueda, D. Puerto, J. Siegel, M. Galvan-Sosa, and J. Solis, *Appl. Surf. Sci.* **258**(23), 9389 (2012).
- ¹⁵K. Waedegaard, M. Frislev, and P. Balling, *Appl. Phys. A* **110**, 601 (2013).
- ¹⁶A. Q. Wu, I. H. Chowdhury, and X. Xu, *Phys. Rev. B* **72**, 085128 (2005).
- ¹⁷P. P. Rajeev, M. Gertsvolf, P. B. Corkum, and D. M. Rayner, *Phys. Rev. Lett.* **102**, 083001 (2009).
- ¹⁸N. Varkentina, N. Sanner, M. Lebugle, M. Sentis, and O. Utéza, *J. Appl. Phys.* **114**, 173105 (2013).
- ¹⁹M. D. Feit, A. M. Komashko, and A. M. Rubenchik, *Appl. Phys. A* **79**, 1657 (2004).
- ²⁰J. R. Peñano, P. Sprangle, B. Hafizi, W. Manheimer, and A. Zigler, *Phys. Rev. E* **72**, 036412 (2005).
- ²¹G. M. Petrov and J. Davis, *J. Phys. B: At., Mol. Opt. Phys.* **41**, 025601 (2008).
- ²²M. Lebugle, N. Sanner, O. Utéza, and M. Sentis, *Appl. Phys. A* **114**, 129 (2014).
- ²³R. Trebino, *Frequency-Resolved Optical Gating: The Measurement of Ultrashort Pulses* (Kluwer Academic Publishers, Dordrecht, The Netherlands, 2002).
- ²⁴J.-C. Diels and W. Rudolph, *Ultrashort Laser Pulse Phenomenon: Fundamentals, Techniques and Applications on a Femtosecond Time Scale* (Academic Press, San Diego, CA, USA, 2006).
- ²⁵N. Sanner, O. Utéza, B. Bussiere, G. Coustiller, A. Leray, T. Itina, and M. Sentis, *Appl. Phys. A* **94**, 889 (2009).
- ²⁶A. Rosenfeld, D. Ashkenasi, H. Varel, M. Wähler, and E. E. B. Campbell, *Appl. Surf. Sci.* **127**, 76 (1998).
- ²⁷K. Sokolowski-Tinten and D. Von der Linde, *Phys. Rev. B* **61**(4), 2643 (2000).
- ²⁸N. M. Bulgakova, R. Stoian, A. Rosenfeld, I. V. Hertel, W. Marine, and E. E. B. Campbell, *Appl. Phys. A* **81**, 345 (2005).
- ²⁹Q. Sun, H. Jiang, Y. Liu, Z. Wu, H. Yang, and Q. Gong, *Opt. Lett.* **30**(3), 320 (2005).
- ³⁰K. Eidmann, J. Meyer-ter-Vehn, T. Schlegel, and S. Hüller, *Phys. Rev. E* **62**(1), 1202 (2000).
- ³¹S. C. Rae, *Opt. Commun.* **97**, 25 (1993).
- ³²A. Couairon and A. Mysyrowicz, *Phys. Rep.* **441**(2), 47 (2007).
- ³³O. Utéza, N. Sanner, B. Chimier, A. Brocas, N. Varkentina, M. Sentis, P. Lassonde, F. Légaré, and J. C. Kieffer, *Appl. Phys. A* **105**, 131 (2011).
- ³⁴J. Hernandez-Rueda, J. Siegel, D. Puerto, M. Galvan-Sosa, W. Gawelda, and J. Solis, *Appl. Phys. A* **112**, 185 (2013).